Ahmad *et al.*
Protection and Control of Modern Power Systems (2022) 7:43
https://doi.org/10.1186/s41601-022-00264-9

Protection and Control of Modern Power Systems

ORIGINAL RESEARCH Open Access

A hybrid circuit breaker with fault current limiter circuit in a VSC-HVDC application

Muhammad Ahmad[1], Chunyang Gong[2], Muhammad Haroon Nadeem[3], Hui Chen[2] and Zhixin Wang[1*]

Abstract

A conventional hybrid circuit breaker (HCB) is used to protect a voltage source converter-based high voltage direct current transmission system (VSC-HVDC) from a short circuit fault. With the increased converter capacity, the DC protection equipment also requires a regular upgrade. This paper adopts a novel type of HCB with a fault current limiter circuit (FCLC), and focuses on the responses of voltage and current during DC faults, which are associated with parameter selection. PSCAD/EMTDC based simulation of a three-terminal VSC-HVDC system confirms the effectiveness and value of HCB with FCLC, by using an equivalent circuit modelling approach. Laboratory experimental tests validate the simulation results. The peak fault current is reduced according to the current limiting inductor (CLI) increase, and can be isolated more quickly. By adopting parallel metal oxide arrester (MOA) with the main branch of HCB, voltage stresses across the breaker components decrease during transient and continuous operation, and less energy needs to be dissipated by the MOA. The remnant current for all cases is transmitted to power dissipating resistor (PDR) in the final stage, and the fault current is reduced to the lowest possible value. When the current from the main branch is transferred to the FCLC branch, transient voltage spikes occur, while smaller PDR is required to absorb current in the final stage.

Keywords: VSC-HVDC, HCB, FCLC, Short circuit fault, MOA

1 Introduction

The expansion of large-scale industry has brought economic growth for many parts of the world, but it simultaneously has caused a severe threat to environment due to the increased carbon dioxide emission. There has been increased use of renewable energy resources for power production and studies have highlighted the critical statistics of renewable energy production. However, these studies also show that there is a gap between renewable energy resources and power generation [1–4]. The apparent reason is that the enriched renewable energy sites are located far from the load centres, and this gives rise to the challenge of transmitting power over long distance. Considering all limitations, HVDC transmission becomes an appropriate technology to connect remote renewable energy with load centres.

The development of HVDC technology has spread over many decades, beginning from mercury rectifiers to VSC [5–8]. A HVDC transmission system can be divided into two major types, i.e., line-commutated converter (LCC-HVDC) and VSC-HVDC [9, 10]. A comprehensive evaluation of both technologies is given in [11]. However, along with the many benefits of VSC-HVDC technology, it has the disadvantage of a fast rising fault current when subject to DC short circuit faults. VSC-HVDC transmission systems employ circuit breakers (CBs) at both sides of the DC line to protect it from short-circuit faults. These breakers can be classified into three major types, i.e., mechanical (MCB), solid state (SSCB), and hybrid (HCB) [12–17]. For the first time, ABB presented the idea of HCB with experimental validation in [18–20]. Later, ALSTOM also proposed a type of HCB [21].

*Correspondence: wangzxin@sjtu.edu.cn

[1] School of Electronics Information and Electrical Engineering, Shanghai Jiao Tong University, Shanghai 200240, People's Republic of China
Full list of author information is available at the end of the article

Various studies have highlighted the performance of HCB [22, 23]. It is concluded that, as the power handling capacity of VSC-HVDC system has increased over the time, the capacity of HCB is inadequate. To improve this situation, a FCLC is used along with a breaker to improve power handling related matters. A FCLC can be divided into two types, i.e., superconducting (SCFCLC) and non-superconducting (NSCFCLC). References [24–27] report some examples of SCFCLC, while [28–32] explain examples of NSCFCLC. The comparative analysis of the two types of FCLC is elaborated in [33]. A FCLC can be used as an independent circuit with a CB [34, 35], while design of the CB can also be associated with FCLC features. References [36, 37] illustrate recent cases with a modified CB. They consider FCLC features, while the limitation of an FCLC is discussed in detail, and the fault current is reduced stepwise.

To match the capacity of a HCB with a VSC-HVDC system, a FCLC can be used with HCB. Some FCLC based HCB or independent FCLC have been proposed, but they contain certain disadvantages [38–40]. One of the major disadvantages of existing FCLC approaches is that some FCLC components remain inside the circuit for both normal and fault conditions. Consequently, it is impossible to increase the value of these components beyond an specific point. Otherwise, it would cost extra losses and possible voltage drop at the receiving side of converter due to heavy inductance. Furthermore, the series and parallel operation of current limiting inductors (CLI) significantly increases the cost and size of the protection equipment. A detailed analysis of the mathematical formulation of fault current is reported in [41, 42]. The studies use a complicated method to estimate the fault current by considering the time-dependent variations of the voltage due to a DC-link capacitor.

A HCB with FCLC is designed by the authors [38], and Fig. 1 shows the structure of the auxiliary branch, where S_1, S_2, S_3...S_n denote the bidirectional switch (BDS) formed by IGBT, while L_1, L_2, L_3...L_n signify the CLI. In normal working condition, the current follows through the low resistive branch. When the system is in a fault situation, current flows through the auxiliary branch. After the fault current has decreased to the desired level in the auxiliary branch, the current is shifted to the fault isolation branch at the terminal stage. Thus, none of the CLI is used in the normal operating condition, so losses due to CLI in the normal condition are negligible, and the numbers and values of CLI can be increased without extra losses.

In Fig. 2, an alternate and more straightforward scheme is developed to evaluate the performance of HCB rigorously. As shown, V_{DC} represents the terminal/source voltage, L_b is the breaker's impedance, also known as current limiting reactance (CLR), L_l is the cumulative line inductance, and R_L is the load resistance. In addition, two different current flow paths are highlighted.

This paper adopts the novel HCB with FCLC proposed in [38], and focuses on the response character of voltage and current. This is associated with the parameter selection of the FCLC. PSCAD/EMTDC-based simulation authenticates the significance of HCB with FCLC by using a three-terminal VSC-HVDC model and an equivalent circuit modelling approach. Laboratory tests validate the simulation results. The main contents of the paper are as follows: Sect. 2 realizes the design and analysis for HCB with FCLC, while Sect. 3 analyses the response behavior of fault current. Section 4 shows the simulation and experimental results, and Sect. 5 contains the conclusions and general commentary on the results.

2 Design and analysis for HCB with FCLC

2.1 Conventional HCB and HCB with FCLC

Figure 3 represents the schematic diagram of conventional HCB without FCLC. This has three branches, i.e., low-resistance, fault current transmission, and fault clearing branches. The CLR, BDS constituted by IGBT, and mechanical switch UFD form the main branch

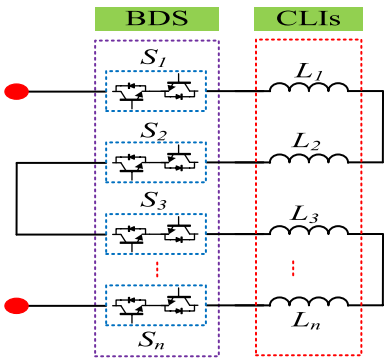

Fig. 1 Structure of the auxiliary branch of HCB with FCLC

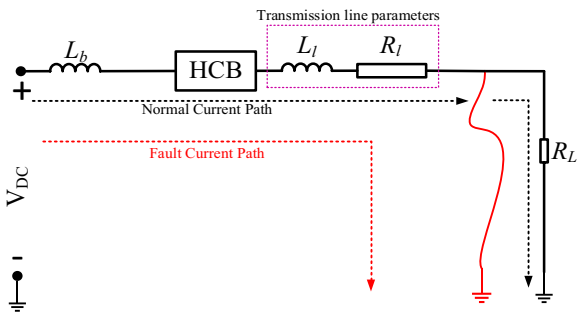

Fig. 2 Representation of equivalent circuit modelling approach

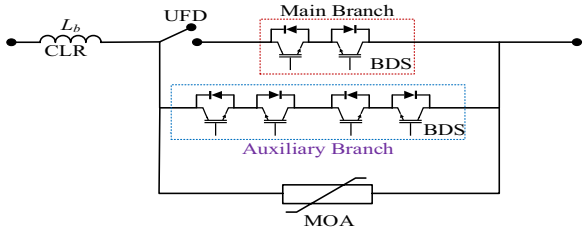

Fig. 3 Schematic diagram of conventional HCB

and the auxiliary branch of the HCB. The third branch, known as the energy absorption branch of the HCB, contains a MOA, which is used for fault elimination.

The current flows through the main branch of the HCB in the normal working condition. After a DC fault and once the fault current crosses a threshold value, it is transferred to the auxiliary branch. At the final stage, the residual current is transferred to the energy absorption branch, isolated from the system, and the UFD can be operated to recover the line physically.

The adopted HCB with FCLC is shown in Fig. 4 [38]. The main and energy absorption branches are the same as the conventional HCB, while the only difference is in the auxiliary branch, as shown in Fig. 4. Similar to a conventional HCB, the current flows through the low resistance main branch during normal operating conditions. When an fault is detected, the fault current is moved to the auxiliary branch, which includes the FCLC. So in this way, the main breaker inductance L_b and FCLC inductance operate in series to suppress the fault current. This causes the fault current to be significantly reduced. Once the desired level of fault current suppression is achieved, the residual fault current is shifted to the MOA in the energy absorption branch for its complete isolation.

2.2 Operating period of HCB

The operating period for each branch of both breakers, i.e., conventional HCB and HCB with FCLC, is shown in Fig. 5, which has two parts. In the first part, various operating stages are described with the association of branches. In the second part, the current and operating

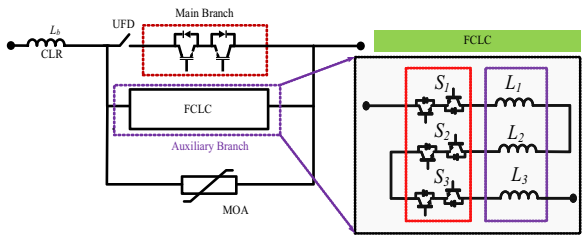

Fig. 4 HCB with FCLC

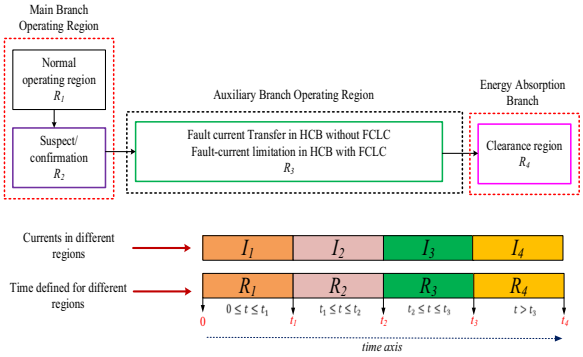

Fig. 5 Operating regions of both breakers

period of each region are explained respectively to show the active branch of the breakers during a particular period.

From Fig. 5, it is apparent that from 0 to t_1, both breakers operate in the normal operating region, which is defined as R_1. The main or low resistive branch of both breakers carries the current I_1, described as the normal or rated current. A fault occurs at t_1, and the fault current begins to increase at a rapid rate from its rated value and reaches the peak point at t_2. It is important to note that during t_1 to t_2, i.e., R_2, the current remains flowing through the main branch for both breakers. This is the transient operating region, and the current during this period reaches the value of I_2. The fault is detected at t_2, and the current flowing path is transferred to the auxiliary branch of both breakers. In fact, the fault current cannot be suppressed through a conventional HCB, and will increase further to the high value during t_2 to t_3, i.e., R_3. In contrast, HCB with FCLC reduces the fault current to a considerable extent, so I_3 is much lower than I_2. The system enters R_4 after t_3, and the residual current for both breakers is switched to the energy absorption branch to be isolated completely.

3 Response behaviour of fault current

There are two most important components used in HCB with FCLC, i.e., CLR and CLI. To optimize the values of inductors used as CLR and CLI, it is crucial to understand the essence of current in various operating stages of the system.

3.1 Response behaviour aroused by short circuit fault

When the system is prone to any types of DC short circuit problem, a complete analysis of the situation considering the comprehensive information of fault current at different stages is required. For the voltage and current characteristics, both simulation and experiment need to

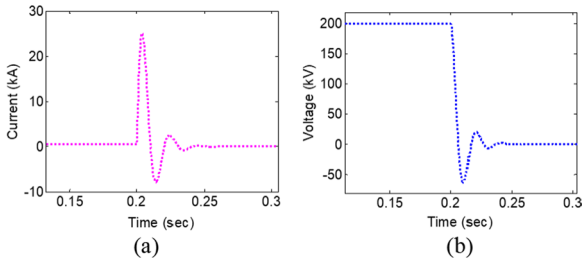

Fig. 6 Voltage and current behavior in fault condition: **a** current; **b** voltage

be noted. A 200 kV voltage level is used for simulation, which is in line with various practical projects, e.g., the Trans Bay Cable project in the US [40].

Based on the parameters in [38], the simulation results are shown in Fig. 6a, b for the current and voltage, respectively. From 0 to 0.2 s, the system operates under normal conditions. The rated current during this stage is 0.5 kA, and the rated voltage is 200 kV. After 0.2 s, the system is subjected to a DC fault, and the fault current escalates at a very fast pace. Conversely, the DC capacitor begins to discharge. Eventually, the capacitor discharges completely, and the voltage and current drop to zero. As L_b and CLI are two critical components used in HCB with FCLC, it is essential to consider some critical points while selecting the appropriate values for these components.

(a) Once the fault in the system is confirmed, the breaker must have the capacity to withstand its peak current value.
(b) The gradual slope of the breaker current should be larger than the slope of the line current.
(c) The fault current must be excluded before the DC-link capacitor begins to discharge.

These points can be analytically summarized as:

$$f(x) = \begin{cases} \max\left(I_{line}\right) < \max\left(I_B\right) \\ \max\left(dI_{line}/dt\right) < \max\left(dI_B/dt\right) \\ t_{fct} < t_{cdt} \end{cases} \quad (1)$$

In (1), $\max(I_{line})$ indicates the peak fault current when subjected to a fault. The maximum value that the breaker can withstand is defined as $\max(I_B)$. dI_b/d_t reflects the breaker current rate of change, and dI_{line}/d_t denotes the line current rate of change. t_{fct} shows the total fault removal time, and t_{cdt} indicates the time taken to discharge the DC-link capacitor.

3.2 Current in different operating regions

To select CLR values in the main branch of both breakers and CLI in the auxiliary branch of HCB with FCLC, it is necessary to establish the equivalent circuits and approximate current in various operating regions. By applying KVL and Laplace transformation, the approximate value of the current can be derived. Figure 7 represents the equivalent circuits in various operating regions, such as R_1, R_2, R_3 and R_4, for both breakers.

Figure 7a represents the circuit during the steady-state operating region, which is defined as R_1 in Fig. 5. The circuit is similar for both breakers. In Fig. 7b, the circuit is effective for the transient operating region, and remains operating until fault detection. The circuit is used in the second operating region for both breakers, which is defined as R_2 in Fig. 5. It is apparent that the circuit shown in Fig. 7b is also used for operating region R_3 for conventional HCB, because no current limiting component is employed to limit the fault. Finally, the circuit in Fig. 7c is used in the operating region, which is defined as R_3 in Fig. 5 for HCB with FCLC.

Applying KVL and Laplace transformation for the circuit in Fig. 7b yields:

$$u(t) = \frac{V_1\omega_0}{\omega_n} e^{-\Upsilon(t-t_1)} sin(\omega_n(t-t_1)+\xi) - \frac{I_1\omega_0}{\omega_n} e^{-\Upsilon(t-t_1)} sin(\omega_n(t-t_1)) \quad (2)$$

$$I_2(t) = -\frac{I_1\omega_0}{\omega_n} e^{-\Upsilon(t-t_1)} sin(\omega_n(t-t_1)-\xi) + \frac{V_1\omega_0}{\omega_n(L_b+L_{Line})} e^{-\Upsilon(t-t_1)} sin(\omega_n(t-t_1)) \quad (3)$$

where $u(t_1) = V_1; I(t_1) = I_1; \xi = R_{Line}/2(L_b+L_{Line})$; $\xi = R_{Line}/2(L_b+L_{Line})$; $\omega_0 = \sqrt{\xi^2+\omega_n^2}$; $\Upsilon = a\tan(\omega_n/\xi)$ and $\omega_n = \sqrt{1/(L_b+L_{Line})C - (R_{Line}/2(L_b+L_{Line}))^2}$.

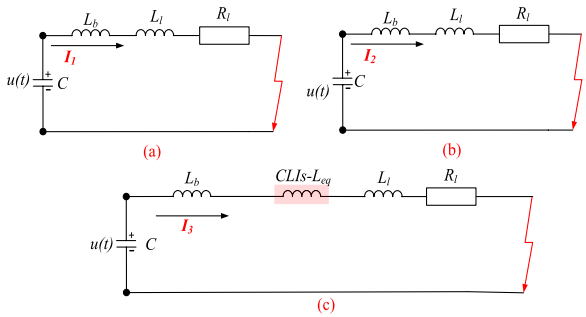

Fig. 7 The equivalent circuits for different operating regions: **a** R_1 for conventional HCB and HCB with FCLC; **b** R_2 and R_3 for conventional HCB, and R_2 for HCB with FCLC; **c** R_3 for HCB with FCLC

This paper studies the fault current with updated parameters and develops a MATLAB algorithm for calculating the values of the CLR. Because of the complex task of estimating the current, a simple and understandable proposition is chosen. Because the voltage fluctuation caused by the DC-link capacitor is low, it is treated as a separate DC source when KVL and Laplace transformation are used for the corresponding circuits in Fig. 7. Thus, during t_1 to t_2, there are:

$$I_1(t) = I_{DC} \tag{4}$$

$$I_2(t) = \delta - (\delta - I(t_1))e^{-\zeta(t-t_1)} \tag{5}$$

$$I_3(t) = \delta - (\delta - I(t_2))e^{-\zeta(t-t_2)} \tag{6}$$

Equations (4)–(6) represent the final results of the current associated with a conventional HCB. In addition, (4) reports the current in normal working condition, which is also defined as the rated current of the system. The results in (5) and (6) are acquired using KVL and Laplace transformation for the circuit in Fig. 7b at two operating regions, R_2 and R_3. In (4), I_{DC} represents the rated DC current of the system. In (5) and (6), different variables are used and are defined as: $\delta = V_1/R_l$, where V_1 represents the terminal DC voltage and R_l is the line resistance; $\zeta = R_l/(L_l + L_b)$, where L_l is the line inductance, L_b is the breaker inductance.

Equations (7)–(9) are obtained for HCB with FCLC by using a similar approach, as:

$$I_1(t) = I_{DC} \tag{7}$$

$$I_2(t) = \delta - (\delta - I(t_1))e^{-\zeta(t-t_1)} \tag{8}$$

$$I_3(t) = \delta - (\delta - I(t_2))e^{-\xi(t-t_2)} \tag{9}$$

Equations (7) and (8) are also acquired from Fig. 7a, b, respectively. For the circuit in Fig. 7c, including the CLI in FCLC, (9) is calculated using KVL and Laplace transformation. An essential point to note is that the structure of HCB with FCLC is modular in nature. As a result, according to design requirements, the number of inductors employed as CLI in FCLC, which are used in the auxiliary branch of the breaker, can be raised or lowered. This paper adopts three CLI as shown in Fig. 4. Moreover, $\xi = R_l/(L_{eq})$, where $L_{eq} = L_1 + L_2 + L_3 + L_l$. L_1, L_2, and L_3 are used as CLI in FCLC.

Based on (5) and (8), a MATLAB program is created to simulate the effect of fault current with various inductance values and fault location from the reference VSC-HVDC system terminal. The effect on I_2 is shown in Fig. 8. This effect is occasioned by inductances,

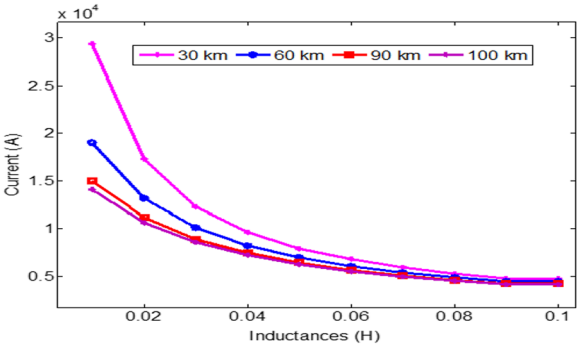

Fig. 8 Impact of varying breaker impedance on current

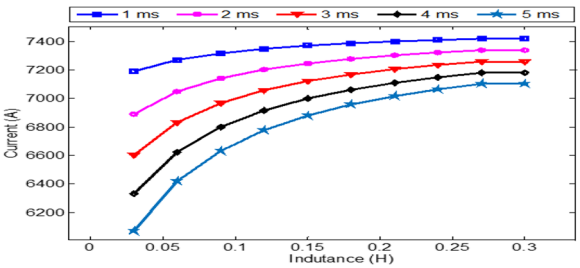

Fig. 9 Influence of CLI on current in R_3

distance between the fault and any reference VSC-HVDC system terminal. It can be observed that the impact of the fault is more extreme if it is closer to the converter station, and the subsequent peak current value is greater. It is clear that if the CLR value in the main branch of both breakers is higher, the rate of current change is lower, and the peak value is also reduced. This paper defines the rated current I_1 as 0.5 kA, rated terminal DC voltage as 200 kV, and 2 ms as R_2. Considering 3.5 kA/ms as the increasing rate of fault current and 100 km as the defecting distance [18], the CLR can be approximated as 38.4 mH.

CLI is elevated using the similar approach for CLR in the main branch. Based on (9), the influence of CLI on the current in R_3 is shown in Fig. 9. There are some important points which have been considered while implementing the algorithm.

(a) Three CLI in FCLC have the same value to avoid mathematical complexities.
(b) In (9), $I(t_2)$ is the current at the previous stage. Considering the rated value of 0.5 kA current, 2 ms of the total operating time in R_2, and 3 kA/ms increasing rate of current, the maximum value of $I(t_2)$ is 7.5 kA.

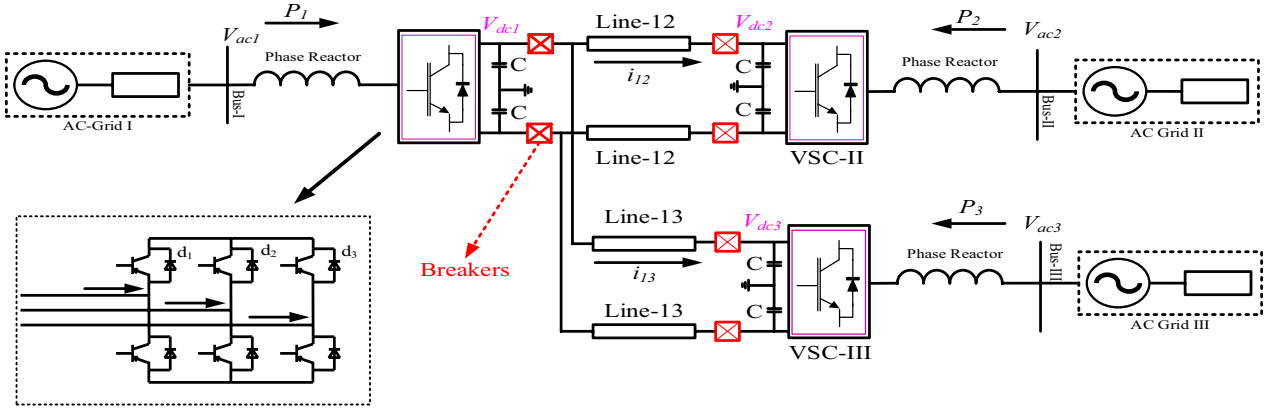

Fig. 10 The three-terminal VSC-HVDC system

Table 1 Parameters of the three-terminal VSC-HVDC system

	Parameter	Value
AC-grid	Grid I voltage/kV	420
	Grid II voltage/kV	420
	Grid III voltage/kV	500
Transmission line	Phase reactor/H	0.0724
	Length of cable 13/km	100
	Resistance per unit length/Ω/km	0.035
	Inductance per unit length/mH/km	0.156
Active power	P_1 for terminal 1/MW	0
	P_2 for terminal 2/MW	200
	P_3 for terminal 3/MW	-200
DC-grid	Rated voltage/kV	400
	Rated current/kA	0.5
	DC link capacitor/μF	300

(c) By assuming the rated terminal DC voltage of 200 kV, the value of L_b is taken as 38.5 mH.

In Fig. 9, the results show that if larger CLI is adopted for a longer period, the fault current is reduced considerably.

4 Simulation and experimental results analysis

4.1 The simulation results

4.1.1 The three-terminal VSC-HVDC system

Figure 10 shows a three-terminal VSC-HVDC system, whose parameters are listed in Table 1 [38]. The DC link voltages for terminal 1, 2, and 3 are V_{dc1}, V_{dc2}, and V_{dc3}, respectively. Similarly, the AC grid voltages for terminal 1, 2, and 3 are denoted by V_{ac1}, V_{ac2}, and V_{ac3}. The flow of current between terminal 1 and 2 is defined as I_{12}, and I_{13} is that between terminal 1 and 3. P_1, P_2, and P_3 represent the active power for terminal 1, 2, and 3, respectively.

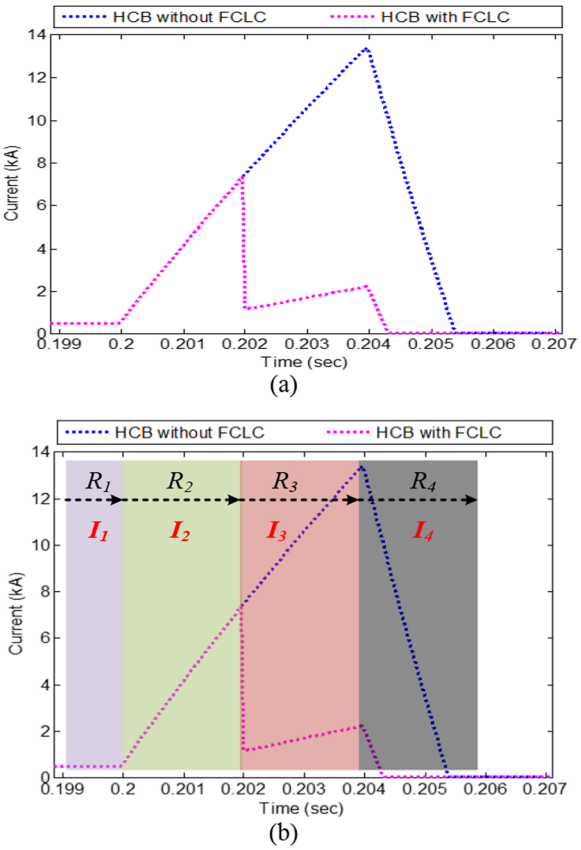

Fig. 11 Response of current under fault condition: **a** no explanation of operating region; **b** with explanation of operating region

Finally, it is noted that the DC power is controlled by adopting a double-loop control strategy.

4.1.2 Response of current

Figure 11 analyses the current when the system is subjected to a DC line-to-line short circuit fault. Figure 11a

reports the basic response, and Fig. 11b highlights the current reaction with an explanation in different operating regions. In Fig. 11a, during 0–0.2 s, the system operates and carries the pre-defined current of 0.5 kA. The current in R_1 is denoted as I_1 in Fig. 11b. At the end of R_1, the fault is injected, and the current rises at the rate of 3.5 kA/ms for both breakers. It is considered that 2 ms is required to detect the fault, so the total span of short period R_2 is 2 ms. At the end of R_2, the current for both breakers has reached the maximum peak value, which is approximately 7.5 kA. Therefore, the current in R_2 is defined as I_2.

We should note that the current I_1 and I_2 in R_1 and R_2 are identical for both breakers in Fig. 11b. The fault is confirmed at the R_2 boundary. For a conventional HCB, no current limiting components are used in the energy transfer/auxiliary branch, and the current I_3 in R_3 keeps rising at the rate of 3.5 kA/ms. Thus, at the end of this region, I_3 reaches almost 14 kA. On the other hand, HCB with FCLC employs three 100 mH CLI in the auxiliary branch. When the system enters R_3, the fault current drops sharply, and reaches the final value of 2 kA at the end of R_3. The residual current in both situations is transferred to the energy absorption branch once the R_3 boundary is passed, and the system enters the last function area R_4. Figure 12 reports the voltage across the breaker, and Fig. 13 depicts the energy dissipated by the MOA.

Figure 12 compares the different responses of voltage for breakers without and with FCLC. The response can be divided into different segments. During 0–0.2 s, the system is in a normal operating state, and zero voltage during this period can be observed across both breakers. The fault is injected at 0.2 s, but the current continues to follow the path of the main branch, i.e., the low resistive path, until 0.202 s. When the current is switched from the main to the auxiliary branch after the current limiting operation starts, a transient voltage

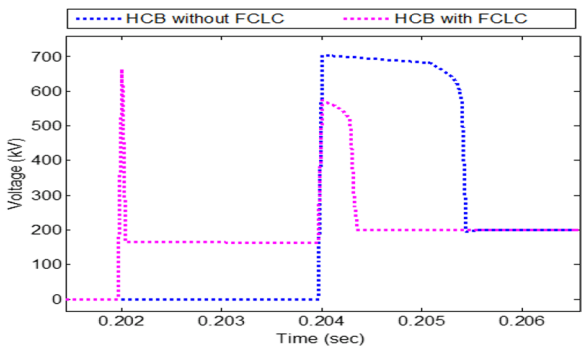

Fig. 12 The voltage across the breaker

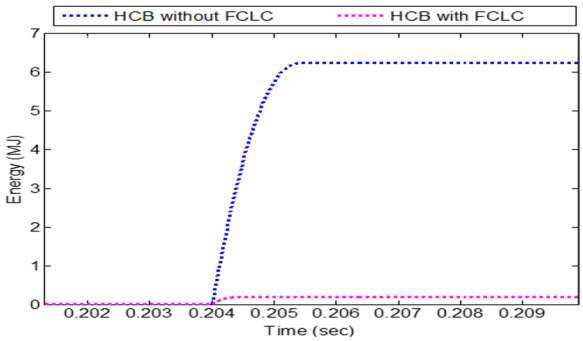

Fig. 13 The power dissipated by MOA

spike is noticed. This is caused by diverging the current flow from one branch to another. However, the voltage returns to the system rating of 200 kV after a short while. When the current is shifted from FCLC to MOA, an similar voltage spike is observed. Figure 13 shows the dissipation of the energy curve under the scope of both breakers. From the response of DC current in Fig. 11, it is evident that at the end of R_3, the peak value of current for conventional HCB is much higher than that of HCB with FCLC. Therefore, the fault current at this stage is quickly removed from the system when HCB with FCLC is adopted. Moreover, less energy is dissipated by MOA in the energy absorption branch. Figure 14 shows an additional result to observe the impact of CLI while the system is subjected to a DC short circuit fault.

Four cases of C1, C2, C3, and C4, with different values of CLI of 100 mH, 150 mH, 200 mH, and 250 mH, respectively, are considered in Fig. 14. It can be seen that if the value of CLI is increased, the peak current in the fault current limiting region R_3 decreases accordingly, and the slope of current in that region also decreases. Also, the fault current can be isolated more quickly.

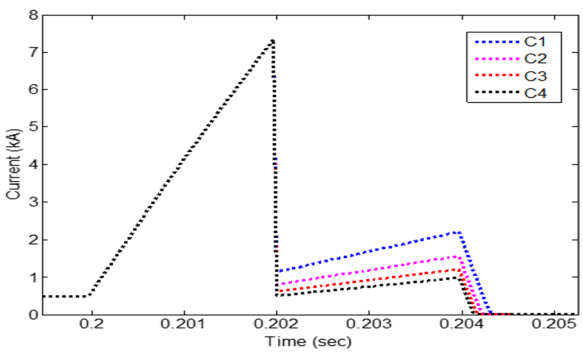

Fig. 14 Impact of CLI on the system current

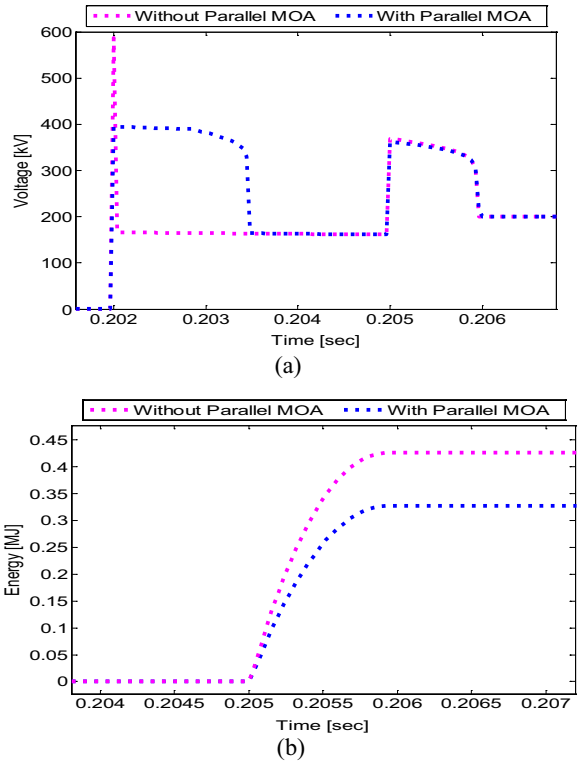

Fig. 15 The result of parallel MOA: **a** voltage, **b** power dissipation by MOA

The impact of parallel MOA is explored and is shown in Fig. 15. Voltage stress across the breaker components decreases with parallel MOA during transient and continuous operation in Fig. 15a, although MOA raises the cost and size of the HCB. In Fig. 15b, parallel MOA is employed with the main branch of HCB, and less energy needs to be dissipated by the MOA at the final stage. In summary, it is noted that a parallel MOA has the greatest influence on voltage and power dissipation.

4.1.3 Comparison among [18, 35, 37] and this paper

Figure 16 displays the conclusions of the comparison analysis. Cases CS1, CS2, CS3 and CS4 represent HCB in [18, 35, 37] and this paper respectively, and the equivalent circuit parameters are listed in Table 2.

All case studies from CS1, CS2, CS3 and CS4 show that the system carries the predefined normal current of 0.5 kA from 0 to 0.2 s. At 0.2 s, a fault is introduced into the system, and the current rises above the rated value of 0.5 kA. Because no fault current limiter is used in CS1, the current continues to rise at a rate of 3.5 kA/ms. After the high fault current is detected at 0.202 s for CS2, CS3, and CS4, the fault current limitation process begins. It can be seen from Fig. 16a that at the end of the fault current limitation period, the fault current for CS4

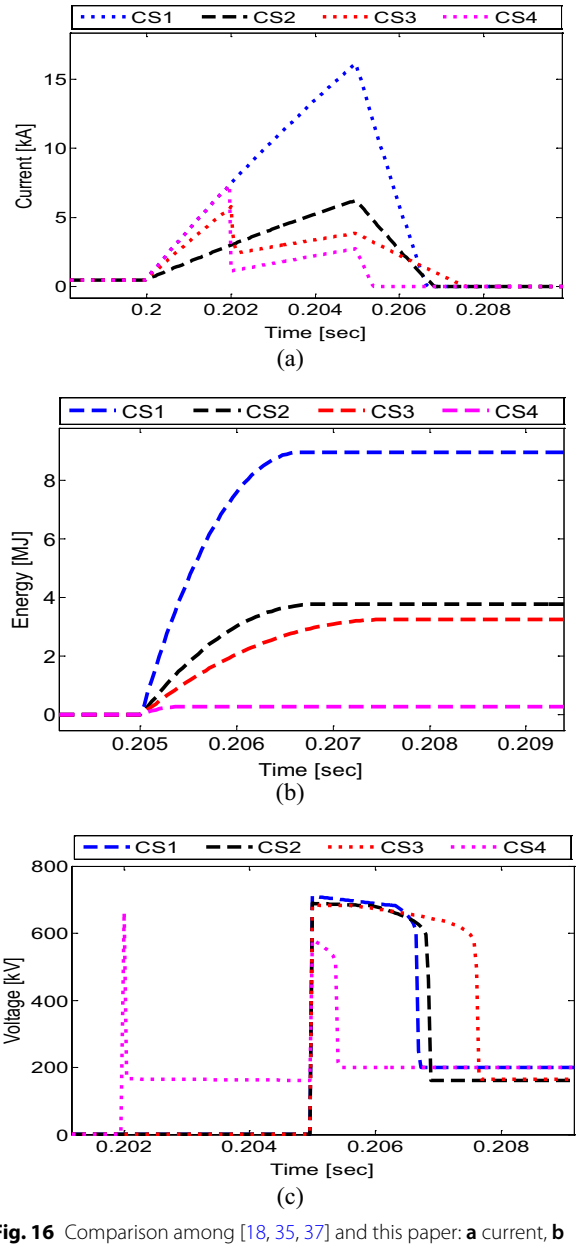

Fig. 16 Comparison among [18, 35, 37] and this paper: **a** current, **b** power dissipation by MOA, **c** voltage

is the lowest compared to other HCBs. Consequently, at the terminal stage for CS4, the least energy is required to be absorbed by the MOA, as can be seen from Fig. 16b. Figure 16c shows the voltage profiles of all breakers. The results show that during normal operating from 0 to 0.2 s, the HCBs have no voltage drop. The transient voltage responses of the HCBs are observed at the instant when the fault current limitation process starts, and at the terminal stage when the fault current is shifted to the MOA. Based on these findings, it is clear that the proposed HCB outperforms its competitors.

Table 2 Equivalent circuit parameters for [18, 35, 37] and this paper

Case study	Parameter	Value
CS1,CS2,CS3,CS4	Terminal voltage (V_{dc})/kV	200
CS1,CS2,CS3,CS4	Line current (I_{dc})/kA	0.5
CS1,CS2,CS3,CS4	Breaker impedance (L_b)/mH	38.4
CS1,CS2,CS3,CS4	Considered distance of fault/km	100
CS1,S2,CS3,CS4	Resistance per unit length/Ω/km	0.035
CS1,CS2,CS3,CS4	Inductance per unit length/mH/km	0.156
CS1,S2,CS3,CS4	Load resistance/Ω	400
CS3	CLIs value ($L_1 = L_2 = L_3$)/mH	100
CS2	HCLC inductance/mH	100
	HCLC resistance/Ω	50
CS4	CLIs value ($L_1 = L_2 = L_3$)/mH	100

Table 3 Parameters for the experimental platform

Component	Value
Breaker inductance L_b/mH	0.3
Rated current/mA	50
PDR/Ω	150
Load resistance R_L/Ω	75
Fault resistance R_f/Ω	10
Shunt resistance R_{shunt}/Ω	10
L_{eqv} in FCLC C1/mH	8.6
L_{eqv} in FCLC C2/mH	9.2
L_{eqv} in FCLC C3/mH	33

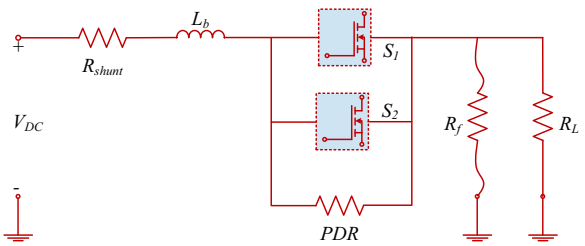

Fig. 17 Circuit for conventional HCB

4.2 Experimental results

4.2.1 Parameters for the experimental platform

Compared to the simulation, the fundamental objective of laboratory experiments is to verify the functionality of the breaker irrespective of rated voltage and current. The rated voltage and current are kept low for the laboratory experiment because of the availability of laboratory equipment and sensitivities associated with the experiment. Thus a small laboratory-scale experimental platform is developed to validate the design of the breakers, and the parameters are listed in Table 3. The circuit used to verify the conventional HCB is shown in Fig. 17.

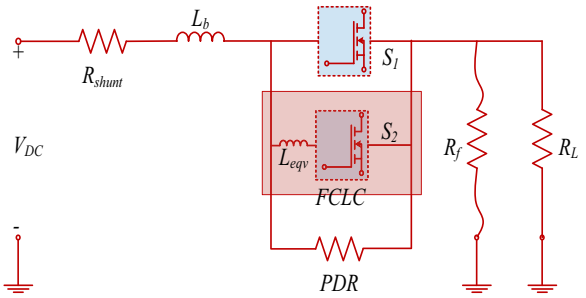

Fig. 18 Circuit for HCB with FCLC

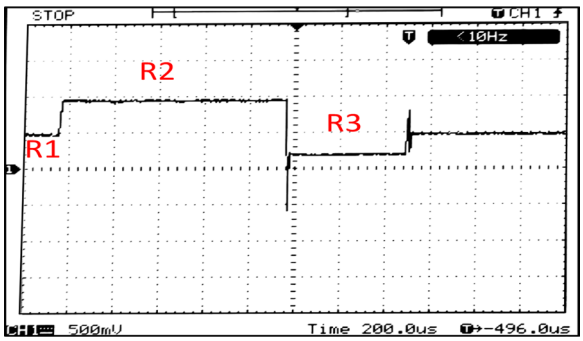

Fig. 19 Current response of conventional HCB

Figure 18 highlights the circuit employed to verify the design of the HCB with FCLC experimentally, which is slightly different from the circuit shown in Fig. 3, to avoid complication and excessive use of circuit components. Line parameters for the experimental platform have been neglected because their values are too small to influence the main experimental results.

An extra resistance R_{shunt} is used with the main branch switch to measure the current by observing the voltage across it. The resistance R_f is used to avoid an extreme rise of fault current, which may be aroused by the DC short circuit connection. A PDR is employed in the energy absorption branch to reduce the residual fault current to the lowest possible value. The MOSFET switches are S_1 and S_2, respectively. An inductance L_{eqv} is also used in Fig. 15 to represent the equivalent value of inductance in Fig. 5. R_L and V_{DC} represent the load resistance and power supply voltage, respectively.

4.2.2 Experimental results

This section verifies and discusses the response of current when the system is subjected to a line-to-line DC short circuit fault, with the current and voltage responses shown in Figs. 19 and 20, respectively. As shown in Fig. 19, the current response is divided into

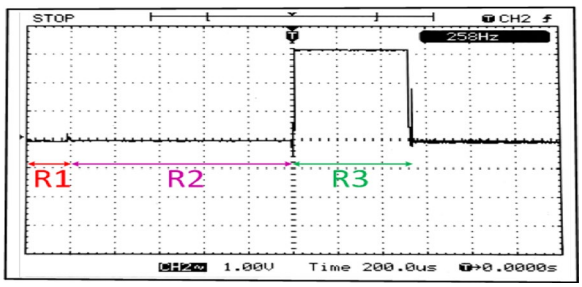

Fig. 20 Voltage response of conventional HCB

three periods. R_1 is associated with the steady-state response of the system. During this time, the system carries 50 mA rated current. When the system is subjected to a line-to-line short circuit fault, the current begins to increase from its rated value and eventually reaches twice the rated value (i.e. 100 mA) and maintains this value during R_2. The reason is that a fault resistance R_f is used, and if this resistance is not employed, the current will increase at the same incremental rate. The fault current is moved to PDR during R_3, and the current reduces dramatically.

In Fig. 20, the voltage response across the breaker is reported. It shows that during R_1 and R_2, there is no voltage increase across the breaker until the fault current is shifted to PDR at the end of the process. The voltage should ideally be equal to the supply voltage of 5 V. However, the results clearly indicate that the value of voltage is just above 3 V. This voltage drop is expected, because of the losses of different connecting wires and internal losses of the switches.

Meanwhile, three results are obtained for the HCB with FCLC at case C1, C2, and C3 as shown in Figs. 21 and 22. In general, the values of FCLC components are dependent on two factors, i.e., the rating of the particular VSC-HVDC project and the level of fault current suppression. Initially, for all three cases, the circuit carries 50 mA current. When the fault occurs, the fault current starts to increase and reaches twice the rated value within seconds for all cases. After that, the system enters the fault limitation stage, and the fault current falls below its peak value of 100 mA because of the CLI in FCLC.

It is interesting to note that the rate of current increase in the fault limitation stage decreases, and the peak value of fault current also decreases before shifting to PDR. This refers to cases C1, C2 and C3. This can also be observed from the results reported in Fig. 21. The remnant current for all cases is transmitted to the PDR in the final stage, and the fault current is reduced to the lowest possible value. If the value of the PDR increases, the current in the final stage can be reduced further. For the previous case when there is no FCLC,

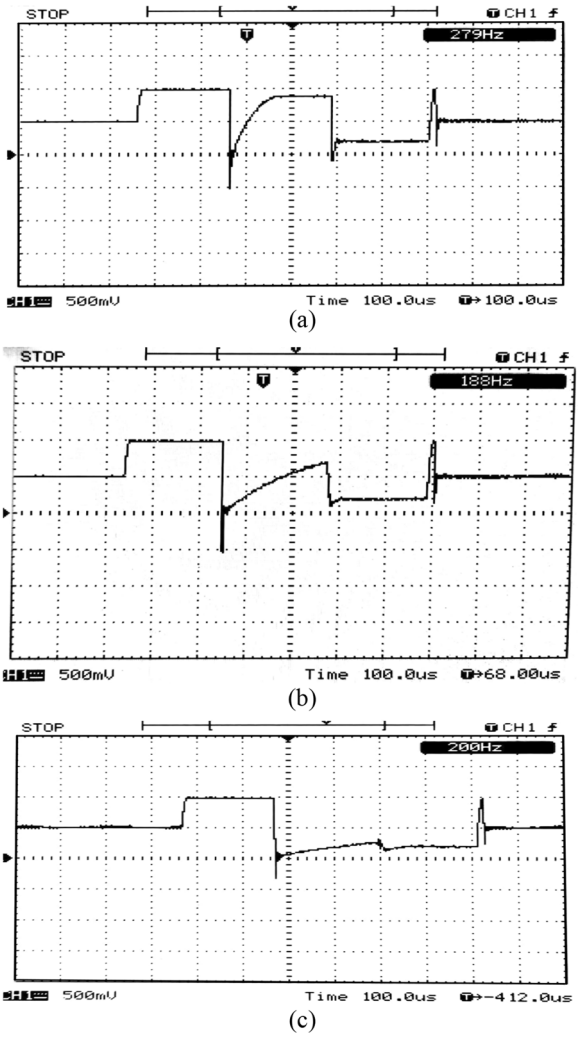

Fig. 21 Current response of HCB with FCLC; **a** case C1, **b** case C2, **c** case C3

the current maintains its peak value of 100 mA before shifting to the PDR, as shown in Fig. 19. It means that the PDR of a conventional HCB needs to absorb higher current in the final stage than PDR of HCB with FCLC.

For the voltage response in the presence of HCB with FCLC shown in Fig. 22, it is observable that there are two voltage spikes. When the current is switched from one branch to another, the spikes occur. The voltage response difference between the conventional HCB and HCB with FCLC is highlighted. When the current from the main branch is transferred to the FCLC branch, the transient voltage spikes occur as shown in Fig. 22. During this stage, a small voltage drop across the breaker is also noticed. For the terminal phase, the response of voltage for both breaker designs remains the same. During this time, the voltage drop should ideally be equal to the supply voltage of 5 V. However, from all

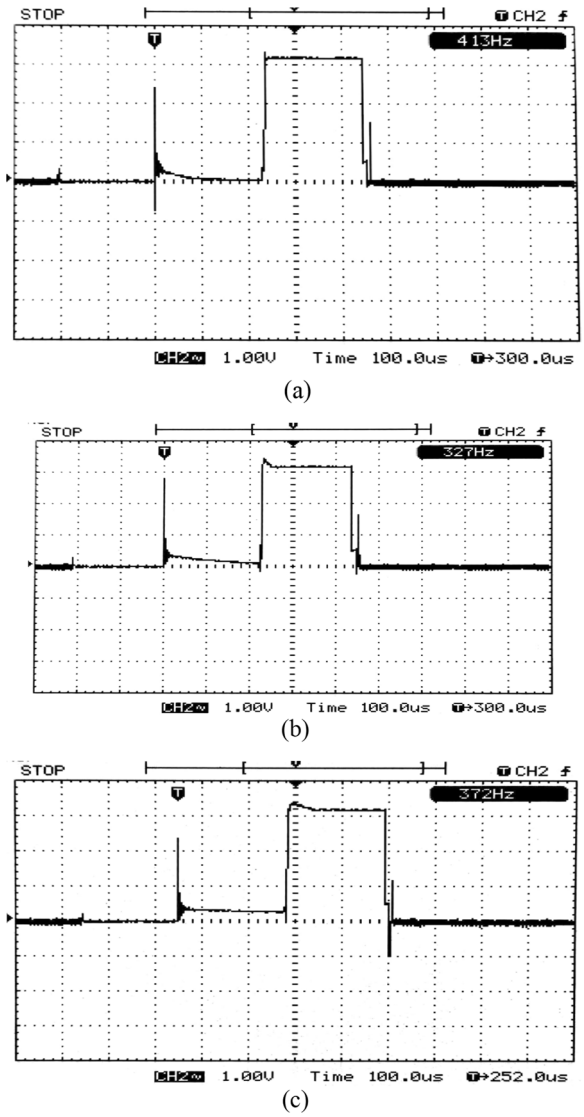

Fig. 22 Voltage response of HCB with FCLC; **a** case C1, **b** case C2, **c** case C3

the results in Fig. 22, it can be seen that the final stage voltage drop across the breaker is 3 V. As previously described, the voltage drop is due to losses of different connecting wires and internal losses of switches.

4.3 Improvement and innovation compared to [38]

This paper focuses on the responses of voltage and current. These are associated with the parameter selection of the FCLC. The comparison between [38] and this paper is listed in Table 4, and the main improvement and innovation over [38] are as follows:

(a) The fault peak current is reduced as CLI increases, of which the slope decreases, and can be isolated more quickly. By adopting a parallel MOA with the main branch of HCB, voltage stresses across the breaker components decrease during transient and continuous operation, and less energy needs to be dissipated by the MOA at the final stage. It is noted that parallel MOA has the greatest influence on voltage and power dissipation.
(b) The experimental results on conventional HCB show that during R_2, fault current increases from its rated value and eventually reaches twice the rated value. It is moved to PDR and reduced dramatically during R_3. The voltage response shows that during R_1 and R_2, there is no voltage increase until the fault current is shifted to PDR at the end of the process.
(c) The experimental results on the HCB with FCLC show that the remnant current for all cases is transmitted to the PDR in the final stage, and the fault current is reduced to the lowest possible value. If the value of PDR increases, the current in the final stage can be reduced further. The voltage response difference between the conventional HCB and HCB with FCLC is highlighted. When the current from the main branch is transferred to the FCLC branch, transient voltage spikes occur. During this stage, a small voltage drop across the breaker is also noticed. The PDR of a conventional HCB needs to absorb considerably more current in the final stage than the PDR of HCB with FCLC.

Table 4 Comparison between [38] and this paper

Nature of comparison	Points of comparison	[38]	This paper
Design and validation	Preliminary design	Yes	Yes
	Transient voltage overshoot components	Yes	No
	Extensive discussion on component selection in FCLC	No	Yes
	Experiment validation of HCB with FCLC	No	Yes
Simulation results	Transient voltage duration	Small	Smaller
	Peak transient voltage	Small	Smaller
	Energy required by MOA to be dissipated at final stage	Less	Lesser

5 Conclusions

The paper focuses on the impact of the FCLC combined with the HCB, and presents the functional features, operating principle, and parameter selection associated with HBC with FCLC. Simulation and laboratory experiments are performed to validate effectiveness. Based on the theoretical discussion, simulation and laboratory experiments, it is concluded that the HCB with FCLC can provide a suitable scheme if large fault current suppression and interruption are required. The following are the conclusions drawn from the results of simulation and experiment:

(a) The fault peak current is reduced as CLI increases, and can be isolated more quickly.
(b) By adopting a parallel MOA with the main branch of the HCB, voltage stresses across the breaker components decrease during transient and continuous operation, and less energy needs to be dissipated by the MOA.
(c) The remnant current for all cases is transmitted to the PDR in the final stage, and the fault current is reduced to the lowest possible value. When the current from the main branch is transferred to the FCLC branch, transient voltage spikes occur, while a smaller PDR is required to absorb current in the final stage.

Abbreviations

BDS: Bi-directional switch; CB: Circuit breaker; CLI: Current limiting inductor; CLR: Current limiting reactance; FCLC: Fault current limiter circuit; HCB: Hybrid circuit breaker; LCC: Line-commutated converter; MCB: Mechanical circuit breaker; MOA: Metal oxide arrester; NSCFCL: Non-superconducting fault current limiter; PDR: Power dissipating resistor; SSCB: Solid state circuit breaker; SCFCL: Superconducting fault current limiter; VSC-HVDC: Voltage source converter-high voltage direct current.

Acknowledgements

The authors would like to express their gratitude to Engr. Muhammad Shafique, who arranged the lab facility at Swedish College of Engineering and Technology, 64200 Rahim yar khan to conduct experiments.

Author contributions

MA: Conception, analytical analysis, simulations, experimental work, and original manuscript write-up. CG: Paper revision, analytical analysis and resources. MHN: Analytical analysis, simulations, and manuscript. HC: Paper revision, and resources. ZW: Supervision, manuscript revision, and resources. All authors read and approved the final manuscript.

Authors' information

Muhammad Ahmad (1991–), male, MSc, Ph.D Fellow, Major in VSC-HVDC Protection.
Chunyang Gong (1991–), male, MSc, Ph.D Fellow and Assistant Researcher, Major in Renewable Energy Generation and Control.
Muhammad Haroon Nadeem (1987–), male, Ph.D, Post. Doc. Fellow, Major in VSC-HVDC Protection.
Hui Chen (1982–), female, Ph.D and Assoc. Prof., Major in Operation and Control of PV Generation.
Zhixin Wang (1964–), male, Ph.D and Prof., Major in MMC based VSC-HVDC and Application.

Funding

This work was supported express by The National Key R&D Program of China (2018YFB1503000, 2018YFB1503001), and The Shanghai Science and Technology Commission Program (20dz1206100).

Availability of data and materials

The relevant data discussed in this paper can only be considered for sharing if a sincere request is extended to the corresponding author.

Declarations

Competing interests

The authors declare that they have no known competing financial interests or personal relationships that could have appeared to influence the work reported in this paper.

Author details

[1]School of Electronics Information and Electrical Engineering, Shanghai Jiao Tong University, Shanghai 200240, People's Republic of China. [2]Shanghai University of Electric Power, Shanghai 200090, People's Republic of China. [3]EnergyVille/Electa Research Group, Electrical Engineering Department ESAT, KU Leuven, 3001 Heverlee, Belgium.

Received: 5 July 2022 Accepted: 20 October 2022
Published online: 05 November 2022

References

1. Quispe, J. C., & Orduña, E. (2022). Transmission line protection challenges influenced by inverter-based resources: A review. *Protection and Control of Modern Power Systems, 7*(3), 406–422. https://doi.org/10.1186/s41601-022-00249-8
2. Moriarty, P., & Honnery, D. (2012). What is the global potential for renewable energy? *Renewable and Sustainable Energy Reviews, 16*(1), 244–252. https://doi.org/10.1016/j.rser.2011.07.151
3. International Renewable Energy Agency (IRENA). (2021). *Renewable capacity statistics 2021*. [Online]. https://www.irena.org/-/media/Files/IRENA/Agency/Publication/2021/Apr/IRENA_RE_Capacity_Statistics_2021.pdf
4. Moriarty, P., & Honnery, D. (2019). Global renewable energy resources and use in 2050. In T. M. Letcher (Ed.), *Managing global warming: An interface of technology and human issues* (pp. 221–235). Elsevier. https://doi.org/10.1016/B978-0-12-814104-5.00006-5.
5. Korytowski, M. (2017). Uno Lamm: The father of HVdc transmission [history]. *IEEE Power Energy Magazine, 15*(5), 92–102. https://doi.org/10.1109/MPE.2017.2711759
6. Long, W., & Nilsson, S. (2007). HVDC transmission: Yesterday and today. *IEEE Power Energy Magazine, 5*(2), 22–31. https://doi.org/10.1109/MPAE.2007.329175
7. Yang, B., Liu, B., Zhou, H., Wang, J., Yao, W., Wu, S., Shu, H., & Ren, Y. (2022). A critical survey of technologies of large offshore wind farm integration: Summary, advances, and perspectives. *Protection and Control of Modern Power Systems, 7*(2), 233–264. https://doi.org/10.1186/s41601-022-00239-w
8. Guarnieri, M. (2013). The alternating evolution of DC power transmission [Historical]. *IEEE Industrial Electronics Magazine, 7*(3), 60–63. https://doi.org/10.1109/MIE.2013.2272238
9. Jovcic, D. (Ed.) (2019). VSC HVDC applications and topologies, performance and cost comparison with LCC HVDC. In *High voltage direct current transmission: Converters, systems and DC grids, second edition* (pp. 137–163). Wiley. https://doi.org/10.1002/9781119566632.ch12.
10. Li, G., Li, C., & Van Hertem, D. (2016). HVDC technology overview. In D. V. Hertem, O. Gomis-Bellmunt, J. Liang (Ed.), *HVDC grids: For offshore and supergrid of the future* (pp. 45–78). Wiley. https://doi.org/10.1002/9781119115243.ch3.

11. Oni, O. E., Davidson, I. E., & Mbangula, K. N. I. (2016). A review of LCC-HVDC and VSC-HVDC technologies and applications. In *2016 IEEE 16th international conference on environment and electrical engineering (EEEIC)* (pp. 1–7). https://doi.org/10.1109/EEEIC.2016.7555677
12. Mohammadi, F., Rouzbehi, K., Hajian, M., Niayesh, K., Gharehpetian, G. B., Saad, H., Ali, M. H., & Sood, V. K. (2021). HVDC circuit breakers: A comprehensive review. *IEEE Transactions on Power Electronics*. https://doi.org/10.1109/TPEL.2021.3073895
13. Du, C., & Wang, C. (2019). Review of DC circuit breaker technology for HVDC application. In *2019 22nd international conference on electrical machines and systems (ICEMS)* (pp. 1–6). https://doi.org/10.1109/ICEMS.2019.8922551
14. Li, G., Liang, J., Balasubramaniam, S., Joseph, T., Ugalde-Loo, C. E., & Jose, K. F. (2017). Frontiers of DC circuit breakers in HVDC and MVDC systems. In *2017 IEEE conference on energy internet and energy system integration (EI2)* (pp. 1–6). https://doi.org/10.1109/EI2.2017.8245743
15. Mokhberdoran, A., Leite, H., Carvalho, A., & Silva, N. (2014). A review on HVDC circuit breakers. In *3rd renewable power generation conference (RPG 2014)* (pp. 5.1.2–5.1.2). https://doi.org/10.1049/cp.2014.0859
16. Franck, C. M. (2011). HVDC circuit breakers: A review identifying future research needs. *IEEE Transactions on Power Delivery, 26*(2), 998–1007. https://doi.org/10.1109/TPWRD.2010.2095889
17. Xu, Q., Huang, X., Chu, X., Li, M., Shuai, Z., Tu, C., & Guerrero, J. M. (2021). Analysis and control of modular multi-terminal DC power flow controller with fault current limiting function. *Journal of Modern Power Systems and Clean Energy, 9*(6), 1375–1385.
18. Hassanpoor, A., Hafner, J., & Jacobson, B. (2015). Technical assessment of load commutation switch in hybrid HVDC Breaker. *IEEE Transactions on Power Electronics, 30*(10), 5393–5400. https://doi.org/10.1109/TPEL.2014.2372815
19. Callavik, M., Blomberg, A., Häfner, J., & Jacobson, B. (2013). Break-through!: ABB's hybrid HVDC breaker, an innovation breakthrough enabling reliable HVDC grids. *ABB Review, 2*, 7–13.
20. Xu, J., Feng, M., & Zhao, C. (2020). Modular reciprocating HVDC circuit breaker with current-limiting and bi-directional series-parallel branch switching capability. *Journal of Modern Power Systems and Clean Energy, 8*(4), 778–786.
21. Nguyen, A.-D., Nguyen, T.-T., & Kim, H.-M. (2016). A comparison of different hybrid direct current circuit breakers for application in HVDC system. *International Journal of Control and Automation, 9*(4), 381–394. https://doi.org/10.14257/ijca.2016.9.4.37
22. Sood, V. K. (2007). HVDC transmission. In M. H. Rashid (Ed.), *Power electronics handbook (second edition)* (pp. 769–795). Elsevier. https://doi.org/10.1016/B978-012088479-7/50048-1.
23. Wang, S., Zhou, J., Shu, J., Liu, T., & Ma, J. (2022). Reclosing current limiting for DC line faults in VSC-HVDC systems. *Journal of Modern Power Systems and Clean Energy, 10*(4), 1040–1049.
24. Chen, L., Zhang, X., Qin, Y., Chen, H., Shen, Q., Xu, Y., Ren, L., & Tang, Y. (2019). Application and design of a resistive-type superconducting fault current limiter for efficient protection of a DC microgrid. *IEEE Transactions on Applied Superconductivity, 29*(2), 1–7. https://doi.org/10.1109/TASC.2018.2882228
25. Lee, H.-Y., Asif, M., Park, K.-H., & Lee, B.-W. (2018). Feasible application study of several types of superconducting fault current limiters in HVDC grids. *IEEE Transactions on Applied Superconductivity, 28*(4), 1–5. https://doi.org/10.1109/TASC.2018.2799745
26. Yang, Q., Le Blond, S., Liang, F., Yuan, W., Zhang, M., & Li, J. (2017). Design and application of superconducting fault current limiter in a multiterminal HVDC system. *IEEE Transactions on Applied Superconductivity, 27*(4), 1–5. https://doi.org/10.1109/TASC.2017.2669152
27. Zhang, L., Shi, J., Wang, Z., Tang, Y., Yang, Z., Ren, L., Yan, S., & Liao, Y. (2017). Application of a novel superconducting fault current limiter in a VSC-HVDC system. *IEEE Transactions on Applied Superconductivity, 27*(4), 1–6. https://doi.org/10.1109/TASC.2017.2656634
28. Chen, S., Li, P., Ball, R., de Palma, J.-F., & Lehman, B. (2015). Analysis of a switched impedance transformer-type nonsuperconducting fault current limiter. *IEEE Transactions on Power Electronics, 30*(4), 1925–1936. https://doi.org/10.1109/TPEL.2014.2329091
29. Tarafdar Hagh, M., Jafari, M., & Naderi, S. B. (2010). Transient stability improvement using non-superconducting fault current limiter. In *2010 1st power electronic & drive systems & technologies conference (PEDSTC)* (pp. 367–370). https://doi.org/10.1109/PEDSTC.2010.5471789
30. Hagh, M. T., & Abapour, M. (2009). Non-superconducting fault current limiters. *European Transactions on Electrical Power, 19*(5), 669–682. https://doi.org/10.1002/etep.247
31. Chen, S., Li, P., Lehman, B., Ball, R., & de Palma, J.-F. (2013). A new topology of bridge-type non-superconducting fault current limiter. In *2013 twenty-eighth annual IEEE applied power electronics conference and exposition (APEC)* (pp. 1465–1472). https://doi.org/10.1109/APEC.2013.6520491
32. Hagh, M. T., Naderi, S. B., & Jafari, M. (2010). New resonance type fault current limiter. In *2010 IEEE international conference on power and energy* (pp. 507–511). https://doi.org/10.1109/PECON.2010.5697635
33. Alam, M., Abido, M., & El-Amin, I. (2018). Fault current limiters in power systems: A comprehensive review. *Energies, 11*(5), 1025. https://doi.org/10.3390/en11051025
34. Huang, Q., Zou, G., Sun, W., & Xu, C. (2020). Fault current limiter for the MMC-based multi-terminal DC grids. *IET Generation, Transmission and Distribution, 14*(16), 3269–3277. https://doi.org/10.1049/iet-gtd.2020.0069
35. Liu, J., Tai, N., Fan, C., & Chen, S. (2017). A hybrid current-limiting circuit for DC line fault in multiterminal VSC-HVDC system. *IEEE Transactions on Industrial Electronics, 64*(7), 5595–5607. https://doi.org/10.1109/TIE.2017.2677311
36. Ahmad, M., Wang, Z., & Zhang, Y. (2020). High-voltage DC circuit breaker with gradual fault-current limitation mechanism for VSC-HVDC applications. *International Transactions on Electrical Energy Systems*. https://doi.org/10.1002/2050-7038.12468
37. Li, S., Zhang, J., Xu, J., & Zhao, C. (2019). A new topology for current limiting HVDC circuit breaker. *International Journal of Electrical Power & Energy Systems, 104*, 933–942. https://doi.org/10.1016/j.ijepes.2018.07.042
38. Ahmad, M., & Wang, Z. (2019). A hybrid DC circuit breaker with fault-current-limiting capability for VSC-HVDC transmission system. *Energies, 12*(12), 2388. https://doi.org/10.3390/en12122388
39. Raza, A., Mustafa, A., Alqasemi, U., Rouzbehi, K., Muzzammel, R., Guobing, S., & Abbas, G. (2021). HVdc circuit breakers: Prospects and challenges. *Applied Science., 11*(11), 5047. https://doi.org/10.3390/app11115047
40. Dekka, A., Yaramasu, V., Fuentes, R. L., & Ronanki, D. (2021). Modular multilevel converters. In E. Kabalcı (Ed.) *Multilevel inverters introduction and emergent topologies* (pp. 147–179). Elsevier. https://doi.org/10.1016/B978-0-12-821668-2.00004-0.
41. Mohan, M., & Vittal, K. P. (2019). DC fault protection in multi-terminal VSC-based HVDC transmission systems with current limiting reactors. *Journal of Electrical Engineering & Technology, 14*(1), 1–12. https://doi.org/10.1007/s42835-018-00027-3
42. Yang, J., Fletcher, J. E., & O'Reilly, J. (2012). Short-circuit and ground fault analyses and location in VSC-based DC network cables. *IEEE Transactions on Industrial Electronics, 59*(10), 3827–3837. https://doi.org/10.1109/TIE.2011.2162712